Journal Pre-proof

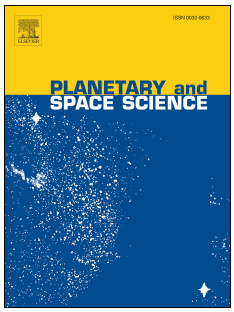

Thermal inertia of Occator's faculae on Ceres

E. Rognini, M.T. Capria, F. Tosi, M.C. De Sanctis, M. Ciarniello, A. Longobardo, F.G. Carrozzo, A. Raponi, M. Formisano, A. Frigeri, E. Palomba, S. Fonte, M. Giardino, E. Ammannito, C.A. Raymond, C.T. Russell

PII: S0032-0633(21)00124-0

DOI: https://doi.org/10.1016/j.pss.2021.105285

Reference: PSS 105285

To appear in: *Planetary and Space Science*

Received Date: 30 January 2020

Revised Date: 9 June 2021

Accepted Date: 13 June 2021

Please cite this article as: Rognini, E., Capria, M.T., Tosi, F., De Sanctis, M.C., Ciarniello, M., Longobardo, A., Carrozzo, F.G., Raponi, A., Formisano, M., Frigeri, A., Palomba, E., Fonte, S., Giardino, M., Ammannito, E., Raymond, C.A., Russell, C.T., Thermal inertia of Occator's faculae on Ceres, *Planetary and Space Science*, https://doi.org/10.1016/j.pss.2021.105285.

This is a PDF file of an article that has undergone enhancements after acceptance, such as the addition of a cover page and metadata, and formatting for readability, but it is not yet the definitive version of record. This version will undergo additional copyediting, typesetting and review before it is published in its final form, but we are providing this version to give early visibility of the article. Please note that, during the production process, errors may be discovered which could affect the content, and all legal disclaimers that apply to the journal pertain.

© 2021 Published by Elsevier Ltd.

Journal Pre-proof

CRediT author statement

Edoardo Rognini: Software, Writing – original draft, Formal analysis

Maria Teresa Capria: Software, Formal analysis

Federico Tosi: Formal analysis

Maria Cristina De Sanctis: Writing - Review & Editing

Mauro Ciarniello: Writing - Review & Editing

Andrea Longobardo: Writing - Review & Editing

Giacomo Carrozzo: Writing - Review & Editing

Andrea Raponi: Writing - Review & Editing

Michelangelo Formisano: Writing - Review & Editing

Alessandro Frigeri: Writing - Review & Editing

Ernesto Palomba: Writing - Review & Editing

Sergio Fonte: Writing - Review & Editing, Data Curation

Marco Giardino: Writing - Review & Editing , Data Curation

Eleonora Ammannito: Writing - Review & Editing

Carol Raymond: Writing - Review & Editing

Christopher Russell: Writing - Review & Editing

Journal Pre-proof

Journal Pre-proof

Thermal inertia of Occator's faculae on Ceres

E. Rognini[1,2], M. T. Capria[3], F. Tosi[3], M. C. De Sanctis[3], M. Ciarniello[3], A. Longobardo[3,4], F. G. Carrozzo[3], A. Raponi[3], M. Formisano[3], A. Frigeri[3], E. Palomba[3], S. Fonte[3], M. Giardino[1], E. Ammannito[5], C. A. Raymond[6], C. T. Russell[7]

Corresponding author: Edoardo Rognini, ASI-SSDC, via del Politecnico snc, I-00133 Rome , Italy. E-mail: *edoardo.rognini@ssdc.asi.it*

[1] ASI Space Science Data Center (SSDC), Via del Politecnico snc, 00133 Rome, Italy

[2] INAF-OAR Osservatorio Astronomico di Roma, Via Frascati 33, 00040, Monte Porzio Catone (RM), Italy

[3] INAF-IAPS Istituto di Astrofisica e Planetologia Spaziali, Via del Fosso del Cavaliere 100, 00133 Rome, Italy

[4] Università Parthenope, DIST, Centro Direzionale Isola C4, I-80143, Napoli, Italy

[5] Agenzia Spaziale Italiana, Via del Politecnico snc, 00133 Rome, Italy

[6] NASA/Jet Propulsion Laboratory and California Institute of Technology, Pasadena, CA, USA

[7] University of California at Los Angeles (UCLA), 90095 Los Angeles, CA, USA

Key points

- The thermal inertia of Occator's faculae on Ceres has been derived using spatially resolved, high resolution VIR data from the Dawn mission.
- In the central part of the Cerealia facula a higher thermal inertia (up to about 60 $Jm^{-2}\ s^{-½}\ K^{-1}$) with respect to the surrounding regions, corresponding to a thermal anomaly, has been derived.

Journal Pre-proof

Abstract

Thermal inertia is a key information to quantify the physical status of a planetary surface; it can be retrieved by comparison between theoretical and observed temperature diurnal profiles. We have calculated the surface temperature for a set of locations on Ceres' surface with a thermophysical model that provides temperature as a function of thermal conductivity and roughness, and we have determined the values of those parameters for which the best fit with the observed data is obtained. The observed temperatures have been retrieved form spatially-resolved data from the Dawn mission. In our previous work [*Rognini et al*., 2019], we have found that the average thermal inertia for the overall surface of Ceres is low (from 1-15 to 60 J m^{-2} $s^{-½}$ K^{-1}), as expected according to the general trend observed in the Solar System for atmosphere-less bodies, while the thermal inertia of the very bright faculae found in the floor of the Occator crater could not be well defined. Using more recently acquired VIR high resolution data we find that the central part of the Cerealia facula displays a thermal anomaly (~ 10 K above the average) compatible with a higher thermal inertia with respect to the surrounding regions, while the Vinalia facula does not display any consequently could have a grain size comparable with the Ceres' surface average.

Keywords: thermal inertia, thermophysical model, Ceres, facula

1. Introduction and background

The dwarf planet Ceres is the largest and most massive body in the Main Asteroid Belt. Its size (mean diameter 939 km) suggests that it has experienced many of the processes typical of planet formation and evolution; its planet-like nature and its survival from the early stages of the Solar System make it an important object for understanding the planetary evolution.

The NASA Dawn mission [*Russell et al*., 2011] was launched in 2007 with the goal of studying Vesta and Ceres, two of the largest bodies of the Main Belt. The Visible and InfraRed (VIR)

mapping spectrometer [*De Sanctis et al.*, 2011] onboard the Dawn spacecraft operates in the overall spectral range 0.25-5.1 μm, with an Instantaneous Field of View (IFOV) of 250 μrad/pixel, and a spectral sampling of 1.8 nm/band in the 0.25-1.0 visual range and 9.8 nm/band in the 1-5 μm infrared range. VIR was designed to provide mineralogical mapping of Vesta and Ceres. Its data are stored as hyperspectral images or "cubes", i.e. bidimensional images of the surface at varying wavelength.

Dawn began orbiting Ceres in March 2015. This phase of the mission was divided in different sub-phases, characterized by different altitudes and related VIR pixel resolution (**Tab. 1**): Rotational Characterization orbit (RC3), Survey, High Altitude Mapping Orbit (HAMO), Low Altitude Mapping Orbit (LAMO) for the nominal mission, plus Extended Mission phases 1 and 2 (XM1 and XM2, with the second extended mission phase following an elliptical orbit). While the primary scientific objective of VIR was to determine and map the surface mineralogy, the long-wavelength component of the infrared spectra in the range 4.5 μm < λ < 5.1 μm can be used to retrieve the surface temperature; the retrieval is applied separately on each pixel unaffected by detector saturation. The VIR instrument can sense temperatures within the uppermost surface layer as thick as tens of microns; in the sampled spectral range the temperature is a non-linear function of radiance, with a larger weight of the hottest sub-pixel features, so the obtained value is representative of the subpixel regions at higher temperatures modulated by their effective areas. Temperature values retrieved in this way show an accuracy better than 3 K above 180 K, and better than 1 K above 210 K, while values below 180 K have increasingly worse accuracy. The lower limit of temperatures sensed by the instrument is dictated by the in-flight instrumental noise, varying over time depending on a number of parameters, most notably the spectrometer's temperature.

Thermal inertia is defined as:

$$TI = \sqrt{k\rho c} \quad (\mathrm{J\ m^{-2}\ s^{-½}\ K^{-1}}) \quad (1)$$

Journal Pre-proof

where k is the thermal conductivity, ρ the density and c the specific heat; it is a fundamental parameter that controls the surface temperature variations of atmosphere-less bodies, and measures the velocity of penetration of the thermal wave controlling the surface temperature. The daily temperature curve of an airless body (i.e., the profile of surface temperature of a given location as a function of the local solar time (LST)), from which thermal inertia can be estimated [e.g., *Neugebauer et al*., 1971; *Audouard et al*., 2014; *Delbo et al*., 2015]), is strongly dependent on the physical and thermal properties of the uppermost surface layer, as thick as few centimeters. Therefore, the derivation of thermal inertia provides an insight into the structure and physical properties of that surface, giving indications on the type (e.g., dust, regolith or rock) and the physical structure of the surface material [*Harris and Lagerros*, 2002].

In a previous work [*Rognini et al.*, 2019], we modeled VIR data acquired during the Survey and HAMO mission phases with an average spatial resolution of 1.1 km/pixel and 0.38 km/pixel, respectively. We derived the average thermal inertia of Ceres and of two specific locations: the crater Haulani and the crater Occator. The average thermal inertia of Ceres turned out to be relatively low (~60 J m^{-2} $s^{-½}$ K^{-1}), which confirms previous independent estimations and is compatible with the trend of the thermal inertia as function of diameter found for the airless bodies of the Main Asteroid Belt [*Delbo and Tanga*, 2008]. Crater Haulani revealed a higher than the average thermal inertia in its central mountainous ridge (up to 130-140 J m^{-2} $s^{-½}$ K^{-1}), corresponding to the most distinct thermal signature on the entire surface of Ceres (Tosi et al., 2018a), which is probably due to the compactness of that particular geologic feature. Conversely, crater Occator, as seen at spatial resolution as high as 0.38 km/pixel, could hardly display any thermal signature, and its surface temperatures could be fitted by theoretical diurnal temperature profiles associated with a broad range of thermal inertia values.

In this work, we follow up our analysis on the bright spots ("faculae") located in crater Occator by using VIR data acquired during the final, elliptical XM2 phase mission at much higher pixel

resolution (9-11 m/pixel). Occator is a 92-km wide crater, centered at 19.7°N 239.6°E. Occator's facula cluster is formed by a very bright spot located in the center of the crater (*Cerealia Facula*), and a secondary group of bright spots in the eastern floor, named *Vinalia Facula*. In particular, Cerealia Facula is the brightest material unit on Ceres with an average visual normal albedo of about 0.6 at a resolution of 1.3 km per pixel (several times Ceres's average) [*Schröder et al.*, 2017; *Longobardo et al*., 2017a]. The spectral slope indicates that the crater interior is younger than the crater walls, and the white material of the faculae is likely even younger: age estimations give 34 ± 2 Ma [*Nathues et al*., 2015] for Occator and 6.9 ± 0.9 Ma for the floor material [*Nathues et al.*, 2016]. Mass deposits originate from the wall of the crater and extend to the floor for 10-20 km, and are covered, at SW and NE, by floor material that extends from the center. The features of these morphological structures, the presence of fractures and their orientation and age, the central depression all suggest post impact processes such as hydrothermal processes, evaporation and emplacement of flow materials [*Jaumann et al.*, 2017]. The spectra of the faculae suggest a composition of a mixture of anhydrous sodium carbonate or natrite (Na_2CO_3) and ammonium chloride (NH_4Cl) or ammonium bicarbonate (NH_4HCO_3) [*Raponi et al*., 2019; *De Sanctis et al*., 2016; *Carrozzo et al*., 2018; *Palomba et al*., 2019]. The faculae probably originated from a relatively recent crystallization of brines that made their way from a subsurface liquid reservoir up to the surface [*De Sanctis et al*., 2016; *Stein et al.*, 2017]. VIR data of the Occator crater acquired on 11, 13, 23 and 24 June 2018, despite their sparse coverage and non-optimal signal-to-noise ratio, first revealed that the central part of the Cerealia facula is about 10 K cooler than the surrounding areas, while Vinalia facula has no thermal contrast compared to the rest of the eastern floor [*Tosi et al.*, 2018b].

Mission phase	**Starting date**	**End date**	**Altitude (km)**	**Pixel resolution (m)**

Journal Pre-proof

RC3		April 23, 2015	May 9, 2015	13,522-13,637	3380-3409
SURVEY		June 6, 2015	June 30, 2015	4380-4423	1095-1106
HAMO		August 17, 2015	October 23, 2015	1450-1475	363-369
LAMO		December 16, 2015	September 2, 2016	355-403	89-101
XM1	XMO1	19 Jun 2016	2 Sep 2016	378	95
	XMO2	10 Oct 2016	04 Nov 2016	1522	380
	XMO3	21 Jan 2017	17 Feb 2017	7738	1930
	XMO4	29 Apr 2017	24 May 2017	19457	4860
XM2		May 21, 2018	July 15, 2018	29-2662	7-665

Table 1. Characteristics of the mission phases of Dawn around Ceres. Data from XM2, i.e. the last mission phase, have been used in this work.

2. Thermophysical analysis of the Occator faculae

2.1 Temperature retrieval method

The method used to derive surface temperatures and spectral emissivity from VIR data is described in details in the Appendix of *Tosi et al.* (2014). It was originally applied to VIR data acquired at Vesta, and subsequently adapted to VIR data acquired at Ceres (Tosi et al., 2018a, 2019a) and to Rosetta/VIRTIS data acquired at the comet 67P/Churyumov-Gerasimenko (Tosi et al., 2019b). Briefly, a synthetic radiance spectrum is computed by summing the solar contribution and the thermal contribution, with emissivity and temperature defined by their respective first guesses. The Kirchhoff's law is used to relate reflectance with emissivity. This is a two-step process: in the first step, spectral emissivity and temperature providing the best fit with the measured spectral radiance within the instrumental error in the 4.5–5.1 μm range (where thermal emission is predominant on most of the dayside) are iteratively and simultaneously computed in a cycle, until convergence around stable values is achieved. In the second step, the scalar value of the surface temperature is retained and a second Bayesian retrieval is performed by considering a broader spectral range

starting 0.5 μm shortward of the crossover point to compute the spectral emissivity up to the upper bound of VIR sensitivity (5.1 μm). Formal errors on the unknown quantities, related to random variations of the signal, are also a standard output of the Bayesian algorithm: each temperature image of Ceres can be associated to an image of the formal errors on the retrieved values, and similarly, for each wavelength where emissivity is retrieved, there is an associated uncertainty. VIR is not sensitive to physical temperatures on the nightside of Ceres, where the signal from the target is considerably low. In VIR data acquired at Ceres, uncertainties increase with decreasing surface temperature, and 170–180 K is the typical minimum temperature value that can still be retrieved while keeping uncertainties < 30 K (typical uncertainties are < 1 K for temperature values > 200 K).

2.2 The Thermophysical Model

The determination of the thermal inertia from measured temperatures requires a thermophysical model [e.g. *Rozitis et al.*, *2011*, *Delbo et al*., 2015]. We have used the one-dimensional model described in Capria et al. (2014) and Rognini et al. (2019), that solves the heat conduction equation and provides the temperature as a function of thermal conductivity, albedo, emissivity, density, and specific heat. The details of the code are reported in the above-mentioned papers; we here briefly recall its main points.

The model is applied to a detailed shape model of Ceres in order to take into account the instantaneous illumination [*Raymond et al*., 2011; *Preusker* et al., 2016]. The code solves with a finite-differences scheme the 1D heat transport equation in all the layers into which the internal radius has been subdivided:

$$\rho c \frac{\partial T}{\partial t} = \frac{\partial}{\partial x}\left(k \frac{\partial T}{\partial x}\right) \quad (1)$$

where ρ is the density, c the specific heat, T the temperature, t the time, x the depth and k is the thermal conductivity. The surface boundary condition is:

159 $$\frac{S(1-A)\mu}{r^2} = X\sigma T^4 + k\frac{\partial T}{\partial x} \quad (2)$$

160 where *S* is the solar constant, *A* is the Bond albedo, μ is the cosine of the solar incidence angle, *r* is
161 the heliocentric distance in AU, σ is the Stefan-Boltzmann constant, and $X = (1 - \varepsilon\xi)\varepsilon$ is a
162 "roughness parameter" where ε is the emissivity and ξ is the sub-pixel roughness. ξ is a measure of
163 the surface irregularity at a scale smaller than the shape model and larger than the thermal skin
164 depth; it can be interpreted, for example, as the percentage of cratered terrain with respect to flat
165 terrain [*Müller and Lagerros*, 1998; *Keihm et al.*, 2012]. Flat surfaces will have ξ values close to 0,
166 while very irregular surfaces will have values approaching unity; moreover, high values of ξ will
167 increase the computed surface temperature, while low values will have an opposite effect. We used
168 an albedo map that has been calculated by conversion of a reflectance map at 1.2 μm [*Ciarniello et*
169 *al*., 2017], this being a good proxy for the reflectance at 0.55 μm (the peak of the solar spectrum),
170 with differences of a few % [*Longobardo et al*., 2019]. It should be noted that, while the bolometric
171 Bond albedo of Ceres at 0.55 μm is 0.037 ± 0.002 on average [*Li et al*., 2019], Occator bright spots
172 have a Bond albedo rising up to 0.24 ± 0.01 through the Dawn Framing Camera clear filter [*Li et*
173 *al.*, 2016], i.e. ~ 6.5 times the Ceres average.

174 The model is applied to a given location specified by planetocentric coordinates (latitude and
175 longitude) referred to a digital shape model of Ceres [*Preusker et al.*, 2016]. The corresponding
176 illumination conditions at any step within a given time interval are derived through SPICE-based
177 software and navigational databases, the so-called "SPICE kernels" [*Acton*, 1996], keeping into
178 account the position of Ceres along its orbit and that of the Dawn spacecraft. Time interval and
179 steps are optimized so as to stabilize the results of the computation.

180 We assume that the surface of Ceres is covered by a layer of particulate material (regolith), ranging
181 from very fine dust to incoherent rocky debris, with density increasing with depth.The formulae for
182 density and thermal conductivity are based on the properties of the particulate material, which have

Journal Pre-proof

been derived from ground and spacecraft observations, lunar in-situ measurements and returned samples [*Capria et al.*, 2014; *Vasavada and Paige*, 1999; *Vasavada et al.*, 2012]. Surface density ranges from 1200 to 1350 kg/m^3 (fine dust and regolith, respectively, see **Tab. 2**) at the surface and increases with depth, while thermal conductivity has the form:

$$k(T) = k_{cond} + k_{rad}T^3 \quad (3)$$

where k_{cond} is the conductive term (that takes into account the conductive heat transfer across the particles) and k_{rad} is the radiative term (that takes into account the radiative heat transfer, sensible at high temperatures). For k_{cond} and k_{rad} we apply the expressions used in *Rognini et al.* (2019), where more details can be found. Laboratory experiments show that the thermal conductivity only depends on the physical structure of the soil and not on composition [*Opeil et al*., 2012]. Three kinds of particulate material have been assumed in this work: fine dust, dust, fine regolith, with the corresponding density profiles (**Tab. 2**). By assuming these materials type, typical total thermal conductivity values (**Eq. 3**) range from about 10^{-5} to 0.001 W m^{-1} K^{-1} (for fine dust and fine regolith, respectively); the lower value is probably unrealistic for our work, and represents a theoretical lower limit in the range we are looking for.

The specific heat for the points located inside the faculae has been set to 1060 J kg^{-1} K^{-1}, which corresponds to the specific heat of sodium carbonate, i.e. the main constituent of the bright faculae. For the points outside the faculae we used a temperature-dependent specific heat derived from a fit of experimental measurements of materials compatible with Ceres surface [*Biele et al*. 2014]:

$$c(T) = a_0 + a_1(T - T_0) + a_2(T - T_0)^2 + a_3(T - T_0)^3 \ \text{(J kg}^{-1}\text{ K}^{-1}\text{)} \quad (4)$$

where $T_0 = 250$ K, $a_0 = 633$ J kg^{-1} K^{-1}, $a_1 = 2.513$ J kg^{-1} K^{-2}, $a_2 = -0.0022$ J kg^{-1} K^{-3}, $a_3 = -2.8 \times 10^{-6}$ J kg^{-1} K^{-4}.

On a real planetary surface, the derivation of thermal inertia is complicated by the presence of small-scale surface roughness, which cannot be detected even in the highest resolution optical

imagery, but should be taken into account to properly model the measured heat flow. In this regard, the problem is degenerate to some extent, because different combinations of parameters, particularly thermal conductivity and surface roughness, in principle might lead to the same value of thermal inertia.

2.2 Derivation of the Thermal Inertia of Cerealia and Vinalia faculae

In order to perform the analysis of the thermal properties of the surface of the Occator faculae we used the procedure already applied to determine the average thermal inertia of Ceres (see *Rognini et al.*, 2019 for a detailed description), while the VIR data used in this work come from the XM2 mission phase (**Tab. 1**). The areas selected and analyzed are reported in **Fig. 1** and **Fig. 2**: the magenta square represents the central part of Cerealia facula, while the cyan square and circle respectively indicate the portion of Occator's floor west of Cerealia facula and the border of the facula itself (**Tab. 3**).

For each VIR pixel, the retrieved temperature value represents the average temperature measured on a resolution cell defined by the instantaneous ground footprint as observed at a given time. For each pixel, a complete set of geometric information, including planetocentric latitude and longitude, and illumination and observation angles, are available. The retrieved temperature values are affected by the illumination geometry, while our thermophysical code, for each surface element approximated by a triangular plate ("facet"), calculates the temperature at zero emission angle (i.e, the local normal to the surface element). To reduce the differences between theoretical and observed temperature values, we then discarded all VIR observations with an emission angle greater than 30°, and uncertainties associated with retrieved temperature values greater than 5 K. For every given area, a set of locations (3-5 points) has been selected in such a way as to cover the area as best as possible, and for every selected location within a given area, we calculated theoretical temperature profiles by assuming varying pairs of k and ξ values. The set of theoretical curves is

231 then compared with the observed temperature data using a chi-square function defined in Rognini et
232 al. (2019), that has to be minimized (for every class of material) as a function of ξ; a thermal inertia
233 value is subsequently derived from thermal conductivity, density and specific heat capacity (Eq. 1).
234 This procedure is based on the fundamental hypothesis that, if for given values of the input
235 parameters the theoretical temperatures match the measured ones within the associated
236 uncertainties, then the input parameters are retained because they are realistic. More precisely,
237 because of the degeneration in roughness-thermal inertia, we identify a range of roughness and
238 thermal conductivities that are candidate "real" values, as they match the observations.

239

Material	**Minimum density (kg/m^3)**	**Maximum density (kg/m^3)**
Fine dust	1200	1800
Dust	1320	1930
Fine regolith	1350	1950

240 **Table 2.** Ranges of density values (in kg/m^3) for the materials considered in this work.

241

Area	**Location (longitude-latitude)**
Cerealia	[239.4°, 239.8°] × [19.4°, 19.8°]
Vinalia	[242.6°, 243°] × [20.2°, 20.4°]
Around Cerealia	[237°, 240.5°]×[18°, 22°] (outside the Z area)

Journal Pre-proof

Table 3. The areas considered in this work. Z is an area defined by $(lon - 239.6°)^2 + (lat - 19.7)^2 \leq 1$.

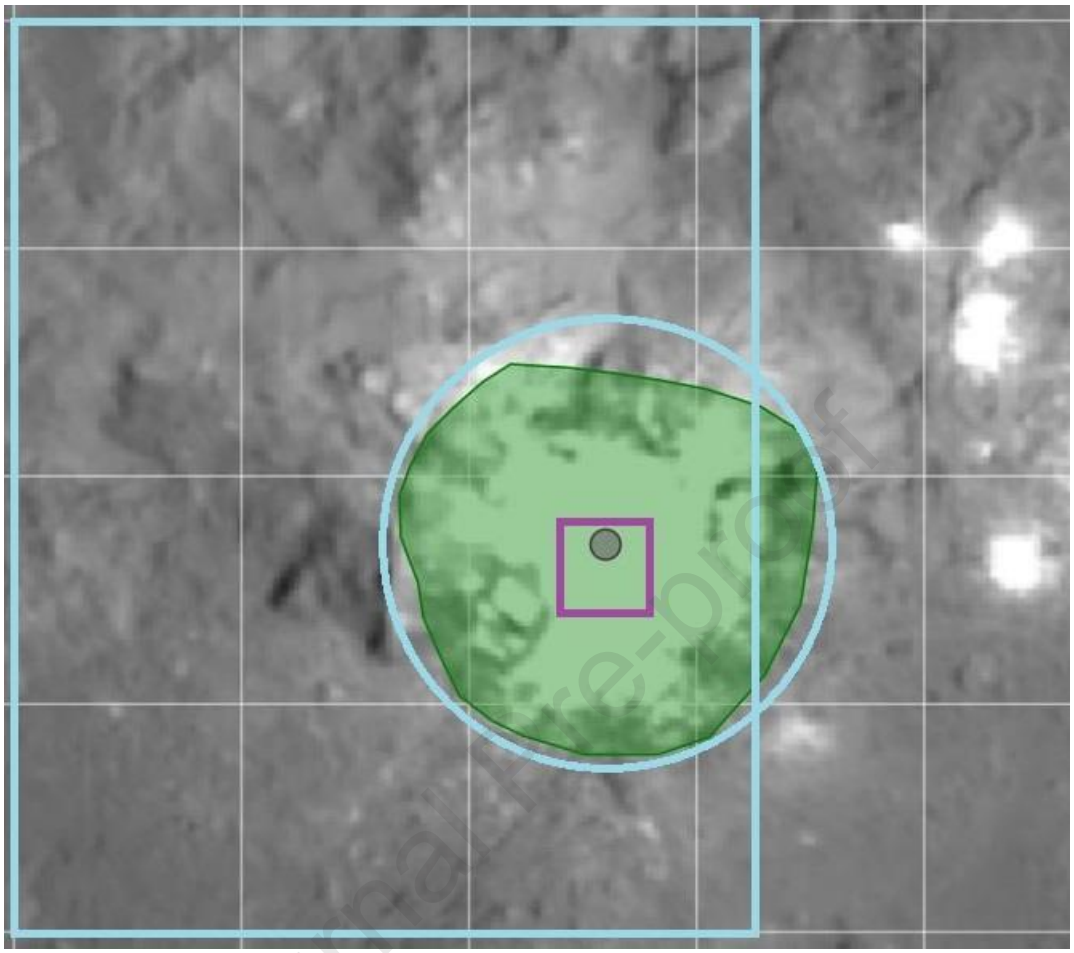

Figure 1. Selected areas for the Cerealia facula and the the surrounding regions (see **Tab. 3**). The square and circle drawn in cyan refer to the area selected around Cerealia, while the magenta square identify the area selected in the central part of Cerealia. The area bordered by the cyan circle and the cyan square is the "Z" area indicated in Tab. 3.

Journal Pre-proof

Journal Pre-proof

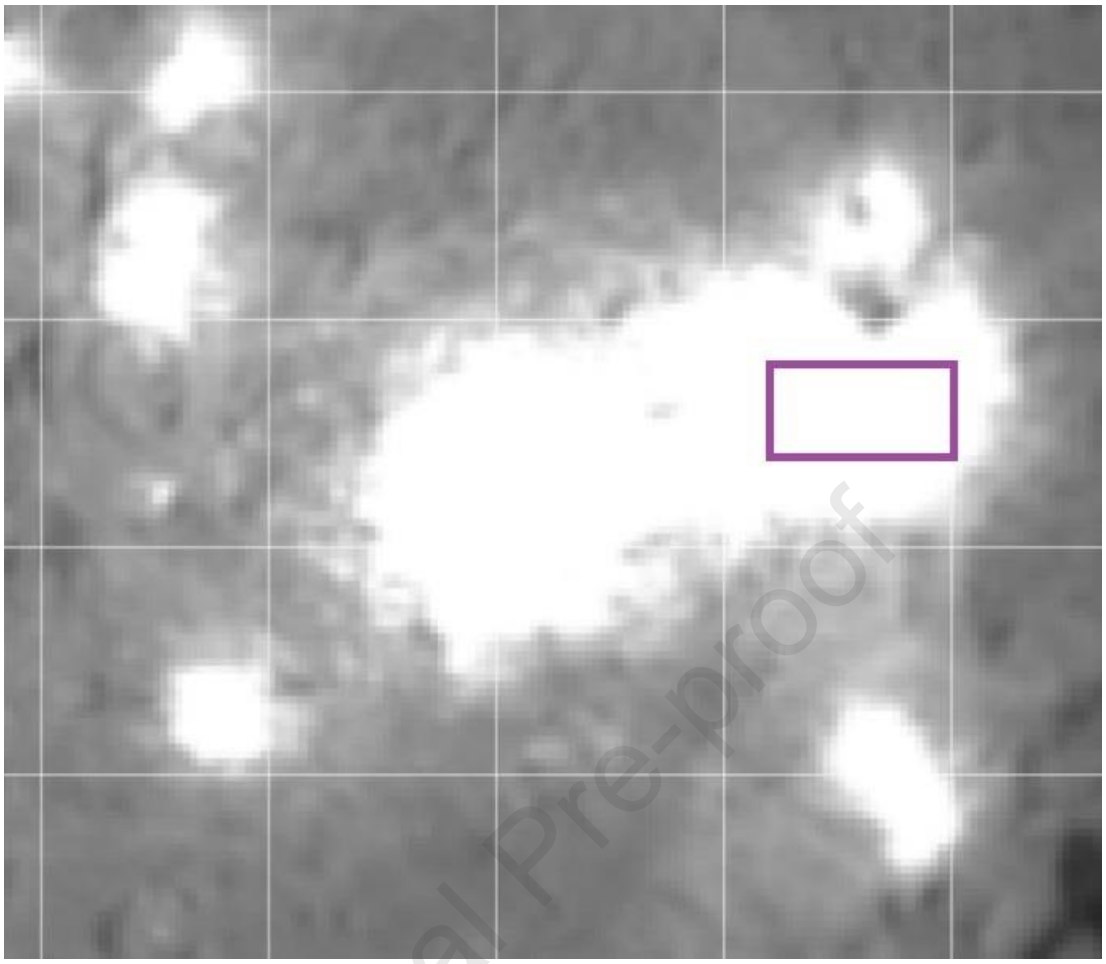

Figure 2. The magenta rectangle surrounds the area selected in Vinalia facula (see **Tab. 3**).

3. Results and Discussion

The results of our analysis are summarized in **Fig. 3**, which shows measured data and modeled diurnal temperature profiles for the central part of Cerealia, a selected region within Vinalia, and a larger area surrounding Cerealia (**Tab. 3**). The temperatures in the central part of Cerealia are lower with respect to those in the surrounding regions, while Vinalia facula does not display any thermal signature. This could indicate a higher thermal inertia only for the inner region of Cerealia facula. A different sub-pixel roughness would also possible, as explained in subsection **2.2**.

Theoretical temperature curves calculated by assuming the material defined as "fine dust", with corresponding thermal inertia up to about 20 J m^{-2} $s^{-½}K^{-1}$, and $\xi \approx 0.3 - 0.4$, fit the observations of both Cerealia and Vinalia faculae; a similar result is obtained by assuming the material defined as

"dust", with thermal inertia up to 55 J m^{-2} $s^{-½}k^{-1}$ and $\xi \approx 0.6 - 0.8$. The curves differ between them only after 11 h LST, when no observed temperature is available, which precludes the possibility to discriminate the most plausible solutions.

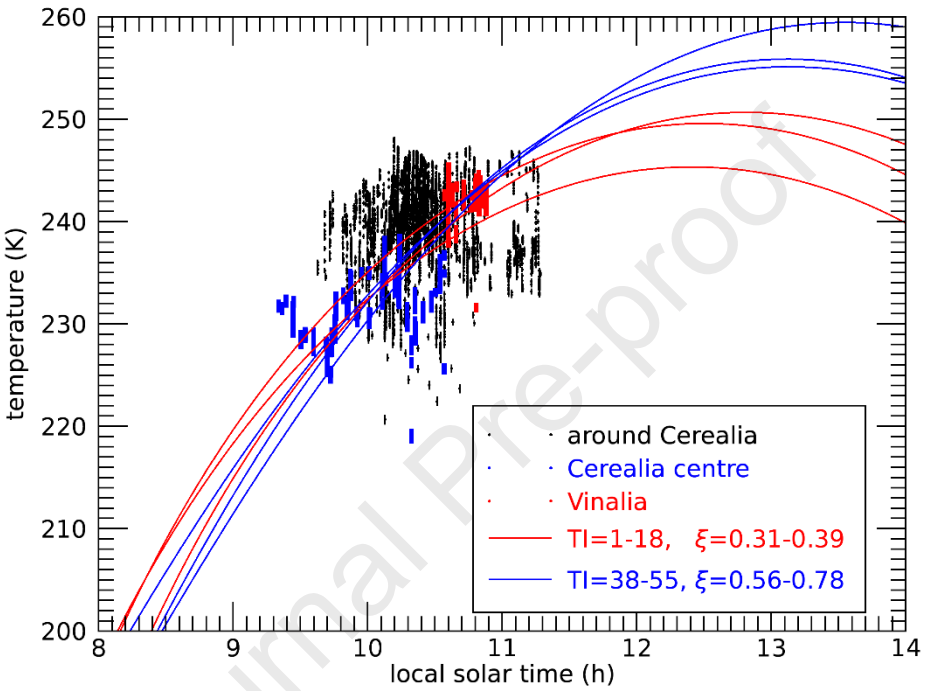

Figure 3. Comparison between observed (points) and theoretical (lines) temperatures in the areas analyzed in this work. The selected areas are reported in **Tab. 3.** For the theoretical temperatures, the corresponding ξ values and the resulting thermal inertia are also shown.

When considering diurnal temperature profiles, the maximum daytime temperature value moves from local noon to the local afternoon with increasing thermal inertia, thus the position of this maximum in principle could further constrain the thermal inertia value. However, due to operational constraints of the Dawn mission, the coverage in terms of local solar time is very limited (typically less than 3 hours in the local morning between 9 and 11.5 h LST, see **Fig. 3**), which precludes this possibility.

Journal Pre-proof

Effects of unresolved surface roughness are important in modeling thermophysical properties of airless bodies. Our model uses the known values of Bond albedo and takes into account the small-scale surface roughness with a simple ξ parameter, rather than considering a variable density of nearly hemispherical concavities at sub-pixel scale, distributed randomly across the surface; the complexity required to implement this approach in our model goes beyond the scope of the article.

To some extent, the thermal conductivity is temperature dependent, and so is the thermal inertia (**Eq. 1**). When the regolith grains are small, the radiative heat transfer is dominant, particularly at high temperatures, because the surface contact between grains is small, and the solid-state heat conduction (transfer by phonons) is less efficient. In this case, the thermal conductivity tends to be small and is very sensitive to the temperature itself, because the radiative heat transfer is proportional to T^3. If the grain size increases then the transfer by phonons becomes dominant, and the conductivity value increases and is less sensitive to the temperature [*Hale & Hapke*, 2002].

In our previous work [*Rognini et al.*, 2019], we found that the surface temperature of the bright spots in crater Occator as seen at a resolution of 0.38 km/pixel could be compatible with both low (1-17 J m^{-2} $s^{-½}$ K^{-1}) and high (up to about 140 J m^{-2} $s^{-½}$ K^{-1}) thermal inertia. Much higher resolution VIR data were needed to highlight a temperature difference in Cerealia facula, which however only shows up in its central part, while Vinalia does not show any thermal contrast at spatial scales ranging from meters to kilometers. *Longobardo et al.* (2017) found that the phase curve of the faculae has the same steepness of the average of Ceres despite their larger albedo. They proposed that this could be due to a mixing of bright and dark material (similar to what happens on Vesta) or a larger grain size and/or a larger roughness. Cerealia facula could have higher thermal inertia with respect to the surrounding regions due to its lower temperature; this hypothesis would agree with the conclusions of *Longobardo et al.* (2017) regarding the larger grain size, because if the grain size increases then thermal inertia increases. A higher roughness value with respect to Ceres' average ($\xi \approx 0.2 - 0.3$, Rognini et al. 2019) is also required in order to fit the temperatures

in this area. The Vinalia data could also be fitted by the high thermal inertia curves, but the fact that no thermal anomaly has been detected in this area suggests that a lower thermal inertia solution, together with a lower roughness value (magenta curve in the **Fig. 3**), appears to be more likely int this case. However, spectral unmixing carried out by *Raponi et al.* (2017) suggests that the grain size of the surface regolith in the faculae could be smaller or anyway compatible with the average grain size of the surface of Ceres; this conclusion would agree with a low thermal inertia solution, especially for Vinalia. Anyway, the roughness value required in order to fit the Vinalia temperatures is higher with respect to the Ceres' average, and this could agree also with the high roughness values suggested by *Longobardo et al.* (2017). The high roughness value could be explained by the young age of Occator: the surface of the faculae has not yet been smoothed because not enough time has passed, and some surface irregularity could still be present today. Moreover, the brines that have reached the surface from the interior are not evenly distributed. *Nathues et al*. (2017) have found that Occator's bright dome formation likely took place over a long period of time, instead than forming in a single event; this different formation could explain the observed differences between the faculae. Unlike Cerealia facula, Vinalia facula is composed of a mixture of carbonate and dark materials (*Palomba et al.*, 2019); the dark component, with a different composition and physical structure with respect to the bright one, could be the reason of a thermal inertia more similar to the average one of the Ceres' surface.

5. Conclusions

We have analyzed the temperature data of the faculae in the Occator crater by using the new high resolution VIR data, acquired in the Extended Mission 2 phase (XM2). The central part of the Cerealia facula displays a thermal anomaly (~ 10 K above the average) compatible with a higher thermal inertia with respect to the surrounding regions; lower values of thermal inertia would also be possible, but because of the temperature anomaly the higher value is the preferred interpretation. This can be supported by other results that seems to suggest larger grain sizes of the surface

regolith. The Vinalia facula does not display a thermal anomaly, and this in consistent with other studies that could indicate a grain size comparable with the Ceres' surface average. The faculae have different history formation and bright/dark material ratio, and this could explain the differences.

Acknowledgments: The VIR project is funded by the Italian Space Agency (ASI), ASI-INAF Contract I/004/12/0. VIR was developed under the leadership of the Istituto di Astrofisica e Planetologia Spaziale (INAF-IAPS), Rome, Italy. The instrument was built by Selex-Galileo, Florence, Italy. Support of the Dawn Science, Instrument, Operations Teams, as well as of the Dawn at Vesta Participating Scientist program, is gratefully acknowledged. We also acknowledge the hard work carried out by Robert Gaskell in providing a detailed shape model that was used in this work to properly model the data. Dawn data are archived in NASA's Planetary Data System; VIR spectral data may be obtained at: https://sbn.psi.edu/pds/resource/dawn/. The computational resources used in this research have been supplied by INAF-IAPS through the DataWell project.

References

Acton, C. H. (1996), Ancillary data services of NASA's Navigation and Ancillary Information Facility, *Planetary and Space Science*, **44**, 65-70

Audouard, J., Poulet, F., Vincendon, M., et al. (2014), Mars surface thermal inertia and heterogeneities from OMEGA/MEX, *Icarus*, **233**, 194–213

Biele, J., Pelivan, I., Kuhrt, E., Davidsson, B., Choukroun, M., Alexander, C. J. (2014), Recommended values and correlations of thermophysical properties for comet modelling, American Geophysical Union, Fall Meeting 2014, abstract id.P41C-3915

Capria, M. T. et al (2014), Vesta surface thermal properties map, *Geophysical Research Letters*, **41**, 1438-1443

Journal Pre-proof

Carrozzo, F. G., de Sanctis, M. C., Raponi, A., Ammannito, E., Castillo-Rogez, J., Ehlmann, B. L., Marchi, S., Stein, N., Ciarniello, M., Tosi, F., Capaccioni, F., Capria, M. T., Fonte, S., Formisano, M., Frigeri, A., Giardino, M., Longobardo, A., Magni, G., Palomba, Zambon, F., Raymond, C. A., & Russell, C. T. (2018). Nature, Formation, and distribution of carbonates on Ceres. *Science Advances*, **4**(3), e1701645. https://doi.org/10.1126/sciadv.1701645

Ciarniello, M., De Sanctis, M. C., et al. (2017), Spectrophotometric properties of dwarf planet Ceres from the VIR spectrometer on board the Dawn mission, *Astronomy & Astrophysics*, **598**, A130

Delbo, M., and P. Tanga (2008), Thermal inertia of main belt asteroids smaller than 100 km from IRAS data, *Planet. Space Sci.*, **257**, 259–265

Delbo, M., Mueller, M., Emery, J. P., Rozitis, B., & Capria, M. T. (2015). Asteroid thermophysical modeling. In P. Michel, et al. (Eds.), *Asteroids IV*, (pp. 107–128). Tucson: Univ. of Arizona. DOI: 10.2458/azu_uapress_9780816532131-ch006

De Sanctis, M. C., et al. (2011), The VIR spectrometer, *Space Sci. Rev.*, **163**, 329–360

De Sanctis, M. C., Raponi, A., Ammannito, E., Ciarniello, M., Toplis, M. J., McSween, H. Y., Castillo-Rogez, J. C., Ehlmann, B. L., Carrozzo, F. G., Marchi, S., & Tosi, F. (2016). Bright carbonate deposits as evidence of aqueous alteration on (1) Ceres. *Nature*, **536**(7614), 54–57. https://doi.org/10.1038/nature18290

Harris, A. W., and J. S. V. Lagerros (2002), Asteroids in the thermal infrared, *in Asteroids III*, edited by W. F. Bottke et al, pp. 205–218, Univ. of Arizona Press, Tucson, Ariz.

Jaumann, R., Preusker., F. et al. (2017), Topography and Geomorphology of the Interior of Occator Crater on Ceres, *EPSC Abstract*, **11**

Journal Pre-proof

371 Keihm, S. J., et al. (2012), Interpretation of combined infrared, submillimeter, and millimeter
372 thermal flux data obtained during the Rosetta fly-by of Asteroid (21) Lutetia, *Icarus*, **221**, 395–404

373 Li, J.-Y. et al. (2016). Surface albedo and spectral variability of Ceres. ApJ **817**, L22, Doi:
374 10.3847/2041-8205/817/2/L22.

375 Li, J.-Y., et al. (2019). Spectrophotometric modeling and mapping of Ceres. Icarus **322**, 144-167.
376 Doi: 10.1016/j.icarus.2018.12.038.

377 Longobardo, A. et al. (2017), Photometry of Ceres and Occator faculae as inferred from VIR/Dawn
378 data, *Icarus*, doi.org/10.1016/j.icarus.2018.02.022

379 Longobardo, A., Palomba, E., Carrozzo, F. G., et al. (2017), Mineralogy of the Occator Quadrangle,
380 *Icarus*, in press, doi: 10.1016/j.icarus.2017.09.022

381 Longobardo, A., Palomba, E., Galiano, A., De Sanctis,M.C., Ciarniello, M., Raponi, A., Tosi, F.,
382 Schröder, S.E., Carrozzo, F.G., Ammannito, E., Zambon, F., Stephan, K., Capria, M.T., Rognini,
383 E., Raymond, C.A., Russell, C.T. (2019). Photometry of Ceres and Occator faculae as inferred from
384 VIR/Dawn data, *Icarus*, **320**, 97-109.

385 Müller, T. G., and J. S. V. Lagerros (1998), Asteroids as far-infrared photometric standards for
386 ISOPHOT, *Astron. Astrophys.*, **338**, 340–352

387 Nathues, A., Hoffmann, M., Schäfer, M., et al. (2015), Sublimation in bright spots on (1) Ceres,
388 *Nature*, **528**, 237

389 Nathues, A., Hoffmann, M., Platz, T., et al. (2016), FC colour images of dwarf planet Ceres reveal a
390 complicated geological history, *Planetary and Space Science*, **134**, 122–127

391 Nathues, A., Platz, T., et al. (2017), Evolution of Occator Crater on (1) Ceres, *Astronomical*
392 *Journal*, **153**, 112

Journal Pre-proof

Neugebauer, G., Münch, G., et al. (1971), Mariner 1969 Infrared Radiometer Results: Temperatures and Thermal Properties of the Martian Surface, *Astronomical Journal*, **76**, 719

Opeil, C. P., Consolmagno, G. J. Et al. (2012), Stony meteorite thermal properties and their relationship with meteorite chemical and physical states, *Meteoritics & Planetary Science*, **47**, 319-329

Palomba, E., Longobardo, A., de Sanctis, M. C., Stein, N. T., Ehlmann, B., Galiano, A., Raponi, A., Ciarniello, M., Ammannito, E., Cloutis, E., Carrozzo, F. G., Capria, M. T., Stephan, K., Zambon, F., Tosi, F., Raymond, C. A., & Russell, C. T. (2019), Compositional differences among Bright Spots on the Ceres surface, Icarus, **320**, 202–212. https://doi.org/10.1016/j.icarus.2017.09.020

Preusker, F., Scholten, F., et al. (2016). Dawn at Ceres — Shape Model and Rotational State. 47th Lunar and Planetary Science Conference, no. 1903

Raponi, A., Carrozzo, F. G., Zambon, F., de Sanctis, M. C., Ciarniello, M., Frigeri, A., Ammannito, E., Tosi, F., Combe, J. P., Longobardo, A., Palomba, E., Pieters, C. M., Raymond, C. A., & Russell, C. T. (2019). Mineralogical mapping of Coniraya quadrangle of the dwarf planet Ceres. *Icarus*, **318**, 99–110. https://doi.org/10.1016/j.icarus.2017.10.023

Raymond, C. A., et al. (2011), The Dawn topography investigation, *Space Sci. Rev.*, **163**, 487–510

Rognini, E., et al. (2019), High thermal inertia zones on Ceres from Dawn data, *Journal of Geophysical Research*, in press. Doi: https://doi.org/10.1029/2018JE005733

Rozitis, B., and Green, S. F., 2011, Directional Characteristics of Thermal-Infrared Beaming from Atmosphereless Planetary Surfaces – A New Thermophysical Model, *Monthly Notices of the Royal Astronomical Society*, **415**, 2042–2062.

Journal Pre-proof

Journal Pre-proof

Russell, C. T., Raymond, C. (2011), The Dawn Mission to Vesta and Ceres, *Space Science Reviews*, **163**, 3-23.

Schröder, S. E., et al. (2017). Resolved spectrophotometric properties of the Ceres surface from Dawn Framing Camera images. Icarus **288**, 201-225. Doi: 10.1016/j.icarus.2017.01.026.

Stein, N. T., Ehlmann, B. L., et al. (2017), The formation and evolution of bright spots on Ceres, *Icarus*, in press, doi: 10.1016/j.icarus.2017.10.014

Tosi, F. et al. (2014). Thermal measurements of dark and bright surface features on Vesta as derived from Dawn/VIR, *Icarus*, **240**, 36-57. Doi: 10.1016/j.icarus.2014.03.017.

Tosi, F. et al. (2018a). Mineralogy and temperature of crater Haulani on Ceres. Meteorit. Planet. Sci. **53** (9), 1902-1924. Doi: 10.1111/maps.13078.

Tosi, F. et al. (2018b). Temperature and emissivity of specific regions of interest on Ceres. European Planetary Science Congress 2018, held 16-21 September 2018 at TU Berlin, Berlin, Germany, id.EPSC2018-555.

Tosi, F. et al. (2019a). Mineralogical analysis of the Ac-H-6 Haulani quadrangle of the dwarf planet Ceres. Icarus **318**, 170-187. Doi: 10.1016/j.icarus.2017.08.012.

Tosi, F. et al. (2019b). The changing temperature of the nucleus of comet 67P induced by morphological and seasonal effects, Nature Astronomy **3** (7), 649-658. Doi: 10.1038/s41550-019-0740-0.

Vasavada, A. R., Paige, D. A. (1999), Near-Surface Temperatures on Mercury and the Moon and the Stability of Polar Ice Deposits, *Icarus*, **141**, 173-193.

Journal Pre-proof

436 Vasavada, A. R. et al. (2012), Lunar equatorial surface temperatures and regolith properties from
437 the Diviner Lunar Radiometer Experiment, *Journal of Geophysical Research*, **117**, E00H18.

Journal Pre-proof

- New high resolution data revealed a thermal anomaly in the center of Cerealia facula
- Higher thermal inertia may be an indicator of higher grain size or cementation
- Faculae are not homogeneous, different evolutionary history may be possible

Journal Pre-proof

Journal Pre-proof

Declaration of interests

☒ The authors declare that they have no known competing financial interests or personal relationships that could have appeared to influence the work reported in this paper.

☐The authors declare the following financial interests/personal relationships which may be considered as potential competing interests:

Journal Pre-proof